



Title	Relationship between Pulmonary Gas Exchange Function and Brain Uptake Dynamics Investigated with Hyperpolarized ^{129}Xe MR Imaging and Spectroscopy in a Murine Model of Chronic Obstructive Pulmonary Disease
Author(s)	Kimura, Atsuomi; Shimokawa, Akihiro; Stewart, Neil J. et al.
Citation	Magnetic Resonance in Medical Sciences. 2024, p. mp.2024-0030
Version Type	VoR
URL	https://hdl.handle.net/11094/100991
rights	This article is licensed under a Creative Commons Attribution-NonCommercial-NoDerivatives 4.0 International License.
Note	




The University of Osaka Institutional Knowledge Archive : OUKA

<https://ir.library.osaka-u.ac.jp/>

The University of Osaka

MAJOR PAPER

Relationship between Pulmonary Gas Exchange Function and Brain Uptake Dynamics Investigated with Hyperpolarized ^{129}Xe MR Imaging and Spectroscopy in a Murine Model of Chronic Obstructive Pulmonary Disease

Atsuomi Kimura^{1*} , Akihiro Shimokawa¹, Neil J. Stewart² , Hirohiko Imai³,
and Hideaki Fujiwara¹ 

Purpose: Chronic obstructive pulmonary disease (COPD) is a complex multisystem disease associated with comorbidities outside the lungs. The aim of this study was to measure changes in metrics of pulmonary gas exchange function and brain tissue metabolism in a mouse model of COPD using hyperpolarized ^{129}Xe (HP ^{129}Xe) MRI/MR spectroscopy (MRS) and investigate the relationship between the metrics of lung and brain.

Methods: COPD phenotypes were induced in 15 mice by 6-week administration of cigarette smoke extract (CSE) and lipopolysaccharide (LPS). A separate negative control (NC) group was formed of 6 mice administered with saline for 6 weeks. After these 6-week administrations, the pulmonary gas exchange function parameter f_D (%) and the rate constant, α (s^{-1}), which are composed of the cerebral blood flow F_i and the longitudinal relaxation rate $1/T_{1i}$ in brain tissue, were evaluated by HP ^{129}Xe MRI/MRS.

Results: The f_D of CSE-LPS mice was significantly lower than that of NC mice, which was in parallel with an increase in bronchial wall thickness. The α in the CSE-LPS mice decreased with the decrease of f_D in contrast to the trend in the NC mice. To further elucidate the opposed trend, the contribution of T_{1i} was separately determined by measuring F_i . The T_{1i} in the CSE-LPS mice was found to correlate negatively with f_D as opposed to the positive trend in the NC mice. The opposite trend in T_{1i} between CSE-LPS and NC mice suggests hypoxia in the brain, which is induced by the impaired oxygen uptake as indicated by the reduced f_D .

Conclusion: This study demonstrates the feasibility of using HP ^{129}Xe MRI/MRS to study pathological mechanisms of brain dysfunction in comorbidities with COPD.

Keywords: brain uptake dynamics, hyperpolarized ^{129}Xe , murine chronic obstructive pulmonary disease, pulmonary gas exchange function

¹Department of Medical Physics and Engineering, Area of Medical Imaging Technology and Science, Division of Health Sciences, Graduate School of Medicine, Osaka University, Suita, Osaka, Japan

²POLARIS, Division of Clinical Medicine, School of Medicine and Population Health, Faculty of Health, University of Sheffield, Sheffield, United Kingdom

³Division of Systems Informatics, Department of Systems Science, Graduate School of Informatics, Kyoto University, Kyoto, Kyoto, Japan

*Corresponding author: Department of Medical Physics and Engineering, Area of Medical Imaging Technology and Science, Division of Health Sciences, Graduate School of Medicine, Osaka University, 2-2 Yamadaoka, Suita, Osaka 565-0871, Japan. Phone: +81-6-6879-2578, E-mail: kimura@sahs.med.osaka-u.ac.jp



This work is licensed under a Creative Commons Attribution-NonCommercial-NoDerivatives International License.

©2024 Japanese Society for Magnetic Resonance in Medicine

Received: March 11, 2024 | Accepted: April 23, 2024

Introduction

Chronic obstructive pulmonary disease (COPD) is a complex multisystem disease associated with a number of extra-pulmonary manifestations including cardiovascular, metabolic, bone, and psychiatric diseases and brain dysfunction.^{1–14} COPD is mainly characterized by pulmonary functional change: in particular, chronic progressive airflow obstruction which causes hypoxia. Decreased oxygen transport to the brain resulting from the hypoxia can lead to brain dysfunction because the brain is highly sensitive to low oxygen supply. Therefore, insights into the effects of COPD-induced pulmonary functional change on brain tissue metabolism may help to elucidate the pathogenic mechanism of brain comorbidities.

However, despite a few reports, for e.g. damage to brain structure,^{4–9} change in cerebral blood volume,¹⁰ and change in cerebral blood flow,^{11–14} investigations of the relationship between change in the lung function and brain tissue metabolism induced by COPD has been limited so far, in large part due to the lack of suitable methodology.

Hyperpolarized ^{129}Xe (HP ^{129}Xe) MRI and MRS are powerful tools for pulmonary function and brain tissue metabolism analyses.^{15,16} Once HP ^{129}Xe is inhaled into the alveolar air space, it partially dissolves in lung tissues and red blood cells with well-separated peaks in chemical shift, allowing the evaluation of gas exchange as well as ventilation function of the lung. In addition, after HP ^{129}Xe dissolves into pulmonary blood, it is transported to the brain and shows characteristic uptake and washout dynamics. By analyzing the brain uptake dynamics of HP ^{129}Xe , it is possible to determine unique brain tissue metabolism metrics such as longitudinal relaxation time in the brain tissue (T_{1i}) as well as global and regional cerebral blood flow (gCBF/rCBF).^{17–20} Since T_{1i} is related to important physiological parameters such as the level of oxygenation,²¹ it is a suitable metric to evaluate the relationship between pulmonary function and brain tissue metabolism.

To make the most of these properties of HP ^{129}Xe , we have developed a preclinical HP ^{129}Xe MRI/MRS system with custom-built flow-mode polarization apparatus to produce HP ^{129}Xe and gas delivery and MR acquisition methodology to evaluate the pulmonary gas exchange and brain tissue metabolism metrics of HP ^{129}Xe .^{17,22–24} Building on our previous studies, in the present study, we attempted to investigate the relationship between pulmonary function and brain tissue metabolism in COPD. Specifically, we measured changes in pulmonary gas exchange function and brain tissue metabolism for the same mice in a mouse model of COPD using HP ^{129}Xe MRI/MRS and investigated the relationship between such metrics.

Materials and Methods

HP ^{129}Xe uptake model

From HP ^{129}Xe MRI and MRS measurements, a set of parameters of the pulmonary gas exchange function, f_D (%), and the brain uptake metric of α (s^{-1}) composed of gCBF and the longitudinal relaxation rate in brain tissue ($1/T_{1i}$) was evaluated as described below. The metric f_D represents the fractional depolarization of HP gaseous-phase ^{129}Xe magnetization due to diffusion of Xe from the alveoli to the lung tissue and blood within a given exchange time (T_{ex}), derived from the xenon polarization transfer contrast method.²⁵ The rate constant, α , in brain tissue can be evaluated by measuring the saturation recovery of HP ^{129}Xe magnetization dissolved in the brain tissue.²³ By substituting F_i measured by ^1H MRI using a pulsed arterial spin labeling (ASL) technique into α , T_{1i} is separately determined.¹⁷ The relationship between these parameters can be expressed as follows.

Under continuous flow condition, the concentration of HP ^{129}Xe within the alveoli reaches a steady state and is represented as a constant, C_A . The HP ^{129}Xe in the alveoli dissolves into pulmonary blood and the concentration of HP ^{129}Xe in the arterial blood, C_a , that reaches the brain tissue is expressed as Eq. (1):

$$C_a = \lambda C_A e^{-t_i/T_{1B}} \quad (1)$$

where λ is the partition coefficient of HP ^{129}Xe between pulmonary blood and gas, t_i is the time required for blood to reach the brain tissue, and T_{1B} is the longitudinal relaxation time of HP ^{129}Xe in the blood.^{23,26}

After complete saturation, the HP ^{129}Xe magnetization in the brain tissue recovers according to its concentration $C_i(\tau)$ of HP ^{129}Xe in the brain depending on the recovery period, τ . The change of C_i is expressed as Eq. (2) from Fick's principle:

$$\frac{dC_i(\tau)}{dt} = F_i C_a - \left(\frac{F_i}{\lambda_i} + \frac{1}{T_{1i}} \right) C_i \quad (2)$$

where λ_i is the partition coefficient between brain tissue and blood. The time-dependent recovery of the signal amplitude of the dissolved-phase HP ^{129}Xe , $S(\tau)$, can be derived by solving Eq. (2) for the initial condition as $C_i(0) = 0$ and analyzed according to Eq. (3):

$$S(\tau) = \eta C_i(\tau) = \frac{\beta}{\alpha} (1 - e^{-\alpha\tau}) \quad (3)$$

$$\text{with } \alpha = \frac{F_i}{\lambda_i} + \frac{1}{T_{1i}}, \quad \beta = \eta F_i \lambda C_A e^{-t_i/T_{1B}},$$

where η is a parameter that normalizes the concentration of HP ^{129}Xe in the brain to the nuclear magnetic resonance (NMR) signal amplitude. When $T_{\text{ex}} \gg L^2/D_{\text{diss}}\pi^2$, where L is the alveolar septum thickness and D_{diss} is the diffusion coefficient of HP ^{129}Xe dissolved in the alveolar septum, the λ term can be expressed using f_D as follows:

$$f_D \frac{V_A}{2V_s} \rightarrow \lambda \quad (4)$$

where V_A is the alveolar gas-space volume and V_s is the alveolar septum volume.²⁷ As is apparent from Eqs. (3) and (4), the saturation recovery of HP ^{129}Xe dissolved in the brain tissue depends not only on α but also on f_D .

Animal Preparation

All experiments complied with the National Institute of Health's Guide for the Care and Use of Laboratory Animals and the Animal Care Guidelines of Osaka University.

A total of twenty one mice – mean age 5 weeks, male, type ddY (Japan SLC, Hamamatsu, Japan) – were divided into two groups: a negative control (NC) group (N = 6 mice) and a CSE-LPS group treated with cigarette smoke extract and lipopolysaccharide (LPS) to induce COPD (N = 15 mice).²⁸ A 20 μL solution of CSE created by bubbling

tobacco smoke (Lark Milds: tar 9 mg, nicotine 0.8 mg; Philip Morris International, New York, NY, USA) into saline (~10 cigarettes per 22 mL) was intra-tracheally administered to each mouse of the CSE-LPS group on five consecutive days within 1 week and repeated on a weekly basis over 6 weeks. On each 5th day, a 20 μL solution of LPS (0.4 mg/kg, Sigma-Aldrich, St. Louis, MO, USA), in saline was intra-tracheally administered once per week over a period of 6 weeks. Saline was administered intra-tracheally to the NC mice following the same schedule as that of the CSE-LPS treated mice. The survival rates of the whole 6 weeks procedure were 100% for the NC group and 87% for the CSE-LPS group (13 out of 15 mice survived).

MR measurements of NC and CSE-LPS groups were performed at 6 weeks after commencing the administration of CSE-LPS, as described below. Prior to MR experiments, mice were anaesthetized with 2% isoflurane (Isoflu®, Dainippon Sumitomo Pharmaceutical, Osaka, Japan) and positioned in a custom-built probe for insertion into the magnet.²⁴ A home-built mouth mask was affixed to the head of the animal for delivery of xenon and oxygen and removal of exhaust gases. A pressure sensor (AD Instruments, Dunedin, New Zealand) was positioned just below the diaphragm to record the respiratory pattern. Warm water was flowed through a rubber tube placed on the abdomen of the mouse to maintain body temperature.

Continuous-flow type production of HP ^{129}Xe

High-purity xenon gas (over 99.995%) with ^{129}Xe in its natural abundance, 26.4%, nitrogen and oxygen were purchased from Air Liquide Japan (Tokyo, Japan).

HP ^{129}Xe was produced by spin-exchange optical pumping method using a home-built continuous-flow type apparatus.²⁴ The gas mixture containing HP ^{129}Xe was delivered to the mouse placed in an NMR probe through the mask attached to the head. In the mask, O_2 was mixed with the Xe/N_2 gas mixture at a rate of 12 mL/min just before inhalation. The mouse inhaled a 56:24:20 volume mixture of $\text{Xe}:\text{N}_2:\text{O}_2$ gases spontaneously.

MRI and MRS

MRI and MRS were carried out after the complete six-week course of NC and CSE-LPS procedures. Immediately before all MR measurements, mice were anesthetized with 2% isoflurane, and non-invasive respiratory-gated imaging was performed without tracheal intubation.

All MR measurements were performed on an Agilent Unity INOVA 400 WB spectrometer (Agilent Technologies, Santa Clara, CA, USA) with a 9.4T vertical magnet (Oxford Instruments, Oxford, UK) and a Highland L-500 Gradient Amp system (Highland Technology, San Francisco, CA, USA). A self-shielded imaging probe with Litz coil, switchable to ^{129}Xe and ^1H frequencies, of 32 mm diameter and 15 mm length (Clear Bore DSI-1117; Doty Scientific, Columbia, SC, USA) was used.

Assessment of pulmonary gas exchange function

The chest of the mouse was fixed at the center of RF coil, then the pulmonary function of gas exchange metric f_D (%) was assessed from HP ^{129}Xe MR images acquired using a balanced steady-state free precession (bSSFP) sequence as described previously.²⁴ Eq. (4) holds when $T_{\text{ex}} \gg L^2/D_{\text{diss}}\pi^2$ as mentioned above. By substituting $L = 4.7 \mu\text{m}$ and $D_{\text{diss}} = 3.3 \times 10^{-6} \text{cm}^2/\text{s}$,²⁹ T_{ex} must be larger than 7 ms. Therefore, T_{ex} was set at 80 ms in this study. A parametric map of f_D of each mouse was calculated by pixel-by-pixel analysis in MATLAB (The MathWorks, Natick, MA, USA). The map was then averaged to obtain a whole lung f_D value. The measurement was repeated three times, and the obtained f_D values were averaged.

Acquisition parameters of HP ^{129}Xe images were as follows: 1000 μs Gaussian-shaped RF pulse of flip angle $\theta = 40^\circ$; acquisition bandwidth, 88 kHz; TR/TE = 3.6 ms/1.8 ms; echo train length, 8; number of shots, 4; number of averages, 8; coronal slice thickness, 20 mm; matrix, 64×32 with an FOV of $80 \times 25 \text{mm}^2$. Acquisition was commenced after confirming a steady state signal by monitoring ^{129}Xe MR spectra obtained by the application of an 8° hard RF pulse with an interval of 2s.

Measurements of HP ^{129}Xe uptake dynamics in the brain

Immediately after the measurement of f_D , uptake dynamics of HP ^{129}Xe in the brain were measured according to the saturation recovery method as previously reported.²³ Briefly, the position of the mouse was changed and the head was set at the center of RF coil. After starting the supply of HP ^{129}Xe to the masked-mouse under a controlled-flow condition, reference NMR spectra were acquired to confirm the steady state of the concentration of HP ^{129}Xe magnetization dissolved in the mouse brain. Then, the HP ^{129}Xe magnetization in the brain was destroyed by applying a chemical-shift selective 90° RF pulse at the center of the dissolved-phase HP ^{129}Xe signal in the brain (196 ppm). After a variable recovery period of τ during which the dissolved-phase HP ^{129}Xe signal arises again from HP ^{129}Xe magnetization that freshly diffuses into the brain from arterial blood, a hard 90° RF pulse was applied to observe the recovered dissolved-phase HP ^{129}Xe signal. The saturation recovery pulse sequence was applied repeatedly with varying τ (0.0, 0.3, 0.6, 1.2, 2.4, 4.8, 9.6, and 19.2 [s]). By nonlinear least-square fitting of the observed signal amplitudes of dissolved-phase HP ^{129}Xe to Eq. (3), we can derive the rate constant, α (s^{-1}), that characterizes signal dynamics of HP ^{129}Xe in the brain. The measurement was repeated three times, and the obtained α values were averaged.

Typical measurement conditions were: spectral band width of 50,000 Hz; number of data points of 32,768; 1000 μs Gaussian-shaped RF pulse and 300 μs hard pulse of flip angle 90° for destroying and observing the dissolved-phase HP ^{129}Xe signal, respectively; number of averages, 8; TR of

0.5s. The data were multiplied by a Lorentzian window function. The spectral assignment was performed by referring to literature data.³⁰ Chemical shifts were referenced to the ^{129}Xe gas signal from the mask at 0 ppm.

Perfusion MRI

Immediately after completion of the HP ^{129}Xe MR measurement of uptake dynamics in the brain, gCBF (F_i) was assessed by ^1H MRI as previously reported¹⁷ for all 6 mice in the NC group and 6 of 13 mice in the CSE-LPS group. In brief, a pulsed arterial spin labeling technique based on a presaturated flow-sensitive alternating inversion recovery (presat-FAIR) with a bSSFP sequence was adopted to assess F_i . The excitation train consisted of a preceding global saturation pulse (sinc pulse, duration = 2 ms) followed by a slice-selective or non-slice-selective inversion pulse (frequency offset corrected inversion inversion pulse, duration 5 ms). The presaturation and inversion pulses were separated by a recovery time of 3.4s. Following the inversion time, TI, of 1.7s which is the time interval between the inversion pulse and the image acquisition, the bSSFP pulse sequence was started. F_i was quantitatively assessed based on tissue magnetization differences between two images acquired with selective inversion and non-selective inversion.^{31,32} The tissue magnetization differences between the two images acquired with the selective inversion (M_{ss}) and the non-selective inversion (M_{ns}) $\Delta M(TI)$ can be written as

$$\begin{aligned}\Delta M(TI) &= M_{ss} - M_{ns} \\ &= 2M_0\alpha_0\lambda \cdot \frac{\exp(-TI/T_{1app}) - \exp(-TI/T_{1a})}{\frac{1}{T_{1a}} - \frac{1}{T_{1app}}} \cdot \frac{F_i}{(1 - \exp(-\tau/T_{1a}))}\end{aligned}\quad (5)$$

where M_0 is the magnetization at equilibrium; α_0 is the inversion efficiency ($\alpha_0 = 1$ for a perfect inversion); λ is the blood/tissue partition coefficient; and F_i is the CBF (measured in mL of blood per 100g of tissue per min, mL/100 g/min). T_{1a} is the longitudinal relaxation time of blood and T_{1app} is the apparent longitudinal tissue relaxation time ($1/T_{1app} = 1/T_1 + F_i/\lambda$, where T_1 is the longitudinal relaxation time of tissue).

Imaging parameters with bSSFP were as follows: 100 kHz spectral band width; a 1000 μs Gaussian-shaped RF pulse; $\theta = 60^\circ$; TR/TE = 4.2 ms/2.1 ms; number of averages = 8; axial slice of 1.0 mm thickness; matrix = 128×128 ; an FOV = $19.2 \times 19.2 \text{ mm}^2$; number of shots = 8; and shot interval = 2.27s. Images with selective inversion were acquired, followed by image acquisition with nonselective inversion. T_{1app} values were evaluated by a slice-selective saturation recovery method (axial slice of 1.0 mm thickness) with 6 values of τ ($\tau = 0.63, 0.9, 1.3, 2.0, 4.0$, and 10s). In the T_{1app} measurements, the bSSFP pulse sequence was also applied to acquire images, where the imaging parameters were identical to those mentioned above except number of averages = 2,

echo train length = 64, and number of shots = 2. T_{1app} maps were obtained by pixel-by-pixel analysis using least-squares fitting based on standard exponential saturation recovery. Then, CBF maps were obtained by solving Eq. (5) with the acquired data. In the analysis, λ was assumed to be 0.9 mL/g,³³ and T_{1a} was set to 2.1s,³² and α_0 was set to 1. CBF values were evaluated by averaging over the whole brain where ROIs were set at the whole brain.

Histology

After perfusion, MRI measurements were completed, the 6 mice in the NC group and the 6 mice in the CSE-LPS group that underwent perfusion imaging were killed with a lethal dose of carbon dioxide gas. Lungs were extracted, immersed in 10% formalin at 25 cmH₂O and processed for histology by staining with hematoxylin and eosin (H&E). Coronal H&E-stained lung images were obtained from each mouse. All digital images were processed using ImageJ (National Institutes of Health, Bethesda, MD, USA). The bronchial wall thickness (h) and mean linear intercept (MLI) were evaluated as previously reported.²⁴

Statistical Analysis

Statistical analysis was performed by Student's t test to identify significant differences between the NC and CSE-LPS groups. All data are presented as mean \pm standard deviation, and differences in functional parameters were considered significant at the $P < 0.05$ level. Finally, we analyzed the correlation among the parameters obtained in NC and CSE-LPS mice using simple regression analysis; $P < 0.05$ was considered statistically significant.

Results

Figure 1 diagrammatically illustrates the relationship between pulmonary gas exchange (f_D) and brain uptake metrics (α and F_i) measured based on the HP ^{129}Xe uptake model. The representative f_D and F_i maps and saturation recovery spectra to derive α are shown.

Figures 2a and 2b show representative f_D maps of the lung and saturation recovery spectroscopy of HP ^{129}Xe signal in the brain of NC and CSE-LPS mice, respectively. The f_D of the CSE-LPS group was significantly decreased compared with that of the NC group as described below. Although the SNR of HP ^{129}Xe spectroscopy in CSE-LPS mice (20.9 ± 8.4) trended to decrease compared to that of NC mice (27.9 ± 7.3), there was no significant difference in the SNR between CSE-LPS and NC mice ($P = 0.10$) (see also Fig. S1 for another example of saturation recovery spectra). In the dissolved-phase spectra in the brain, a single dominant peak was consistently observed at around 196 ppm for both of the CSE-LPS and NC mice and attributed to the signal originating from HP ^{129}Xe dissolved in the brain parenchyma.^{17,30} A weak peak at around 188 ppm was identified as ^{129}Xe dissolved in non-brain tissue. The origin of the shoulder peak

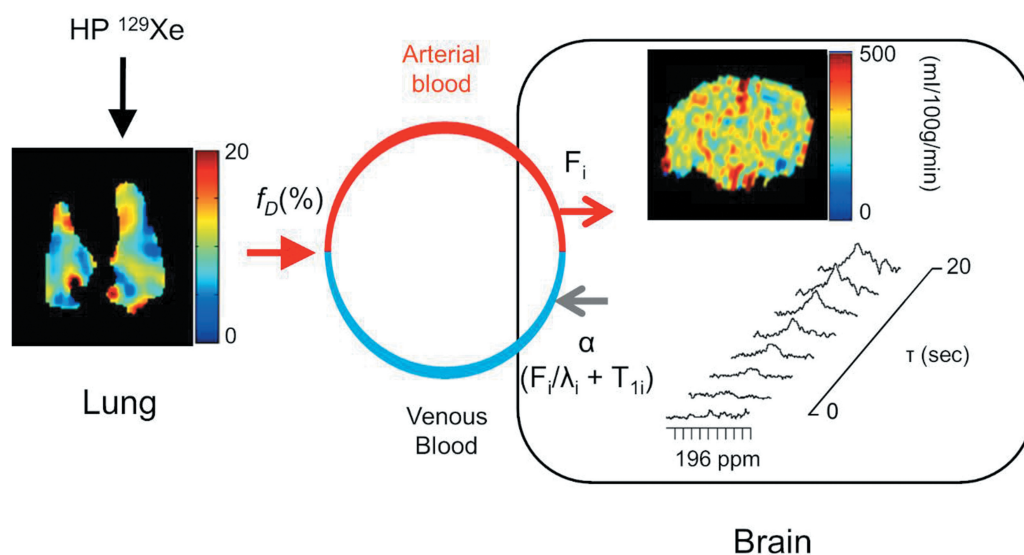


Fig. 1 Relationship between pulmonary gas exchange (f_D) and brain uptake function (α and F_i) measured based on the HP ^{129}Xe uptake model. HP ^{129}Xe , hyperpolarized ^{129}Xe .

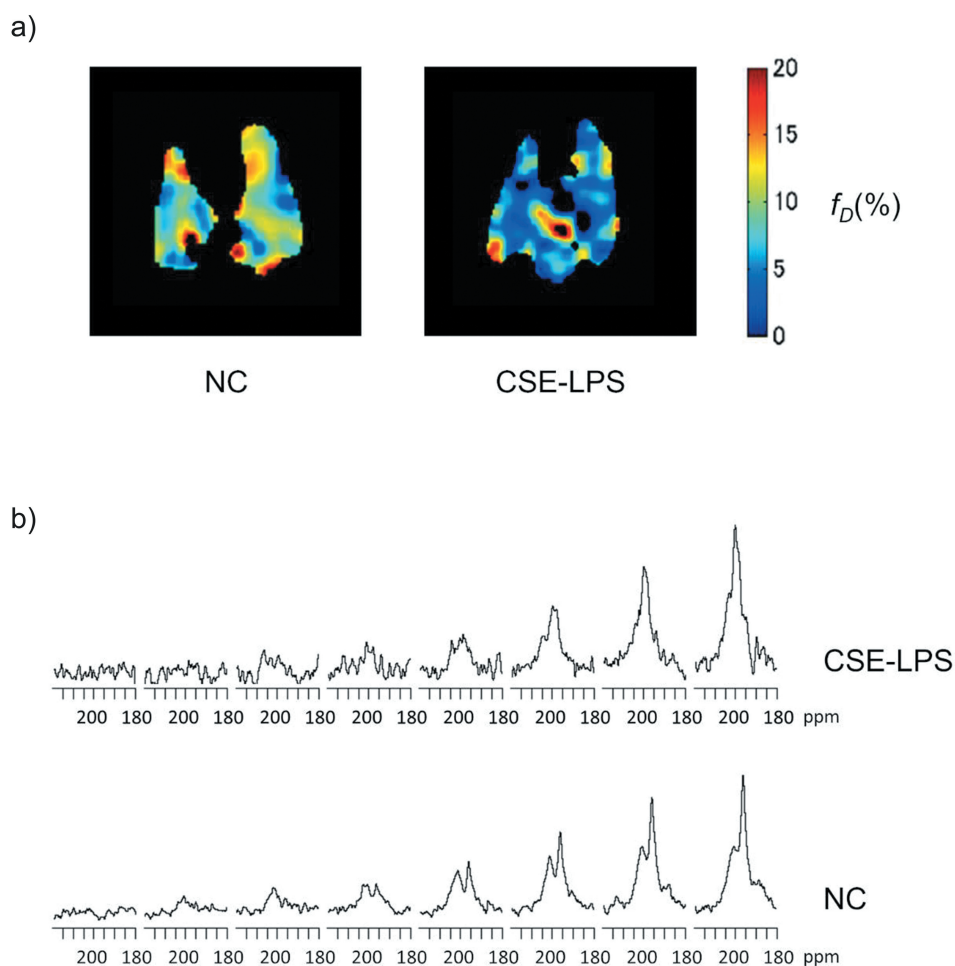


Fig. 2 Example f_D maps evaluated by HP ^{129}Xe MRI (a) and profiles of saturation recovery of HP ^{129}Xe in brain (b) of NC and CSE-LPS mice. The f_D values were 6.9% for NC mouse and 4.4% for CSE-LPS mouse, respectively. CSE-LPS, cigarette smoke extract and lipopolysaccharide; HP ^{129}Xe , hyperpolarized ^{129}Xe ; NC, negative control.

Table 1 Experimentally determined metrics of f_D , α , F_i , and T_{1i} of NC mice*

NC				
Mouse	f_D (%)	α (s ⁻¹)	F_i (mL/100 g/min)	T_{1i} (s)
1	5.5 (1.1)	0.119 (0.023)	178	12.5
2	6.1 (1.0)	0.110 (0.023)	179	14.1
3	6.4 (1.0)	0.111 (0.017)	220	15.9
4	6.9 (0.8)	0.103 (0.033)	182	15.9
5	6.0 (0.7)	0.119 (0.013)	193	13.0
6	6.8 (1.1)	0.096 (0.013)	197	18.9
Mean (SD)	6.3 (0.5)	0.110 (0.009)	192 (16)	15.1 (2.4)

*Values of f_D and α represent the mean \pm SD for measurements repeated three times. NC, negative control; SD, standard deviation.

around 202 ppm is still unknown although it may be attributed to ¹²⁹Xe dissolved in blood.³⁴ The intensity of the peak around 196 ppm was used to derive the α value.

Tables 1 and 2 lists the experimentally determined metrics of f_D , α , and F_i of NC and CSE-LPS groups, respectively. T_{1i} was calculated by substituting α and F_i into Eq. (3), in which λ_i was evaluated as 0.76 based on the method described in Ref. 35 with hematocrit of 47% and temperature of 37°C. The average f_D value of the CSE-LPS group ($f_{D, CSE\&LPS} = 4.4 \pm 0.8\%$) was significantly reduced ($P < 0.01$) compared with that of the NC group ($f_{D, NC} = 6.3 \pm 0.5\%$) whereas there were no significant differences in α , F_i and T_{1i} values between the CSE-LPS and NC groups. Figure 3 shows comparison of f_D , α , F_i , and T_{1i} between the CSE-LPS and NC mice obtained from Tables 1 and 2.

Figure 4a shows representative histological microphotographs obtained from the lungs of NC and CSE-LPS mice. Figure 4b shows the boxplots of bronchial wall thickness (h) of the NC and CSE-LPS mice. The bronchial wall of CSE-LPS group was significantly thickened ($h_{CSE\&LPS} = 16.3 \pm 2.0 \mu\text{m}$) compared with that of NC group ($h_{NC} = 10.2 \pm 1.4 \mu\text{m}$) by the 6 weeks CSE-LPS administration procedure ($P < 0.01$). There was no significant difference in MLI between the CSE-LPS ($MLI_{CSE-LPS} = 40.9 \pm 3.7 \mu\text{m}$) and NC ($MLI_{NC} = 40.6 \pm 3.9 \mu\text{m}$) mice. Figure 4c shows the correlation between bronchial wall thickness and pulmonary gas exchange function ($f_D(\%)$) of the NC and CSE-LPS mice.

Figures 5–7 summarizes the correlations between pulmonary gas exchange (f_D) and brain uptake metrics (α , F_i , and T_{1i}), respectively. Figure S2 in the supporting information shows

Table 2 Experimentally determined metrics of f_D , α , F_i , and T_{1i} of CSE-LPS mice*

CSE-LPS				
Mouse	f_D (%)	α (s ⁻¹)	F_i (mL/100 g/min)	T_{1i} (s)
1	6.0 (1.0)	0.144 (0.031)	235	10.8
2	4.7 (1.0)	0.109 (0.004)	213	16.1
3	4.4 (0.9)	0.101 (0.009)	197	17.2
4	3.3 (0.9)	0.092 (0.021)	189	19.7
5	3.5 (0.7)	0.096 (0.010)	180	17.7
6	4.0 (0.9)	0.101 (0.021)	196	17.2
7	4.7 (0.6)	0.109 (0.024)		
8	4.7 (0.7)	0.112 (0.011)		
9	5.2 (1.0)	0.122 (0.025)		
10	4.6 (0.8)	0.131 (0.019)		
11	3.3 (0.6)	0.105 (0.026)		
12	4.2 (0.9)	0.107 (0.031)		
13	4.9 (0.9)	0.121 (0.016)		
Mean(SD)	4.4 (0.8)	0.112 (0.015)	203 (20)	16.0 (3.7)

*Values of f_D and α represent the mean \pm SD for measurements repeated three times. CSE-LPS, cigarette smoke extract and lipopolysaccharide; NC, negative control; SD, standard deviation.

the correlations between brain uptake parameters; α , F_i , and T_{1i} . While significant correlations exist between the parameters obtained from CSE-LPS mice, it is not the case for NC mice.

Discussion

COPD phenotype induced by CSE and LPS

Previously, we reported that combined administration of cigarette smoke (CS) and LPS could induce a COPD phenotype in mice; confirmed by bronchial wall thickening after 6 weeks administration and emphysema after 10 weeks administration.²⁴ Similarly, in the present study, bronchial wall thickening was confirmed to be induced by the combined administration of CSE and LPS for 6 weeks (Figs. 4a

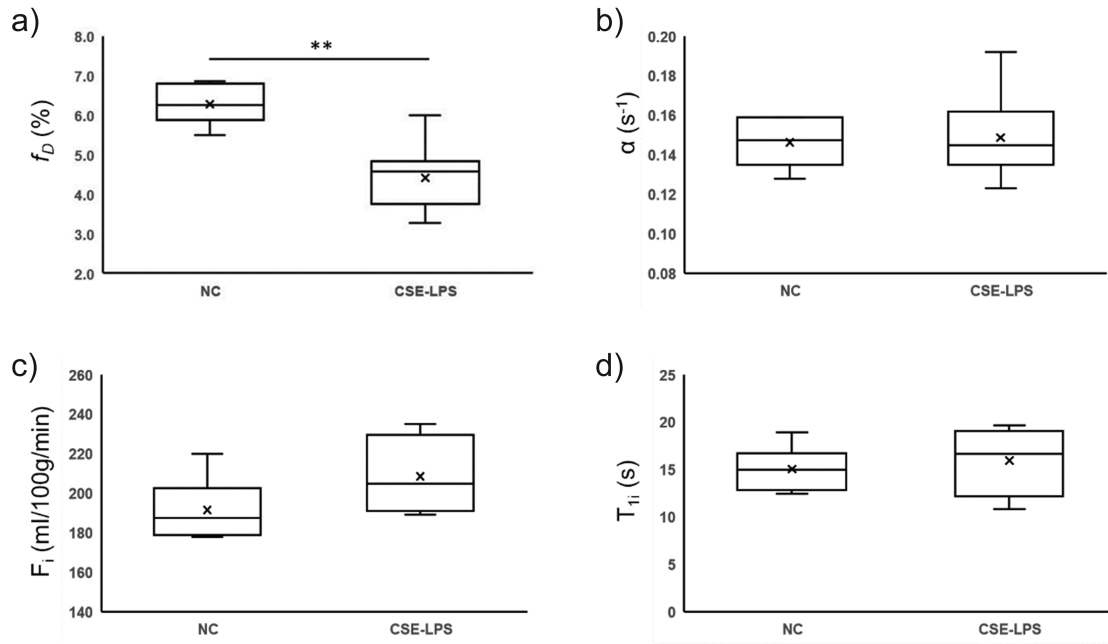


Fig. 3 Box plots of comparison of f_D (a), α (b), F_i (c), and T_{1i} (d) between CSE-LPS and NC mice (**: $P < 0.01$). CSE-LPS, cigarette smoke extract and lipopolysaccharide; NC, negative control.

and 4b), resulting in air flow obstruction and decreased gas exchange function (Figs. 2a and 3a). The bronchial wall thickening was negatively correlated with the pulmonary gas exchange function (f_D (%)), indicating that the f_D decreased as the symptoms became severe (Fig. 4c). The use of CSE has also been reported to develop a mouse model of tobacco addiction³⁶ and is likely more appropriate than the use of CS for investigating the effects of CS on the brain.

Characteristics of brain functional parameters of HP ^{129}Xe

By evaluating the metrics of pulmonary gas exchange function, f_D (%), the rate constant, α (s^{-1}), and gCBF, F_i (ml/100 g tissue/min), in the brain using MRI/MRS, the relationship between lung function and the intracerebral dynamics of HP ^{129}Xe could be investigated (Fig. 1). No significant difference in α was observed between the CSE-LPS mice and the NC mice, whereas there was a significant difference in f_D (Figs. 2b and 3b, Tables 1 and 2).

Here, it should be noted that α is a composite parameter composed of F_i and T_{1i} , and its interpretation is not straightforward. Therefore, F_i was measured independently using perfusion MRI to derive T_{1i} in this study. As a result, for the NC mice, a strong negative correlation was observed between T_{1i} and α while no correlations were found between F_i and α and F_i and T_{1i} (Figure S2). That is, for the NC mice, the change of α is dependent on the change of T_{1i} while it is independent on the change of F_i . On the other hand, for the CSE-LPS mice, strong correlations were found between all

parameters (F_i and α , T_{1i} and α , and F_i and T_{1i}). In other words, certain changes occur in the lung and brain metrics in a certain direction in the CSE-LPS mice. Since T_{1i} changes depending on blood oxygen saturation and oxygen concentration in brain tissue,^{37–39} the above results suggest that changes in oxygen concentration resulting from F_i change due to the COPD pathology could also be detected.

Interrelation of f_D and α

Despite the significant decrease of f_D in the CSE-LPS group compared to that in the NC group, no significant difference was observed in α as mentioned above. Therefore, the correlation between f_D and α was investigated. As a result, opposing trends were observed in the NC and CSE-LPS groups (Fig. 5). That is, a negative correlation was observed between f_D and α in the NC group; by contrast, a positive correlation was observed in the CSE-LPS group. In Fig. 5, for many individual mice in the CSE-LPS group, α was similar to that of the NC group although f_D was significantly reduced. However, 4 out of 13 mice in the CSE-LPS group showed significantly higher α values than the NC mice, and correspondingly the f_D values of these mice were not significantly lower than those of the NC group. Therefore, this is suggestive that α was increased in mild COPD and decreased in severe COPD as lung function declines further.

Insights into mode of propagation of dysfunction from lung to brain

From these preliminary results, the meaning of α of the CSE-LPS mice is shown to be different from that of the NC mice.

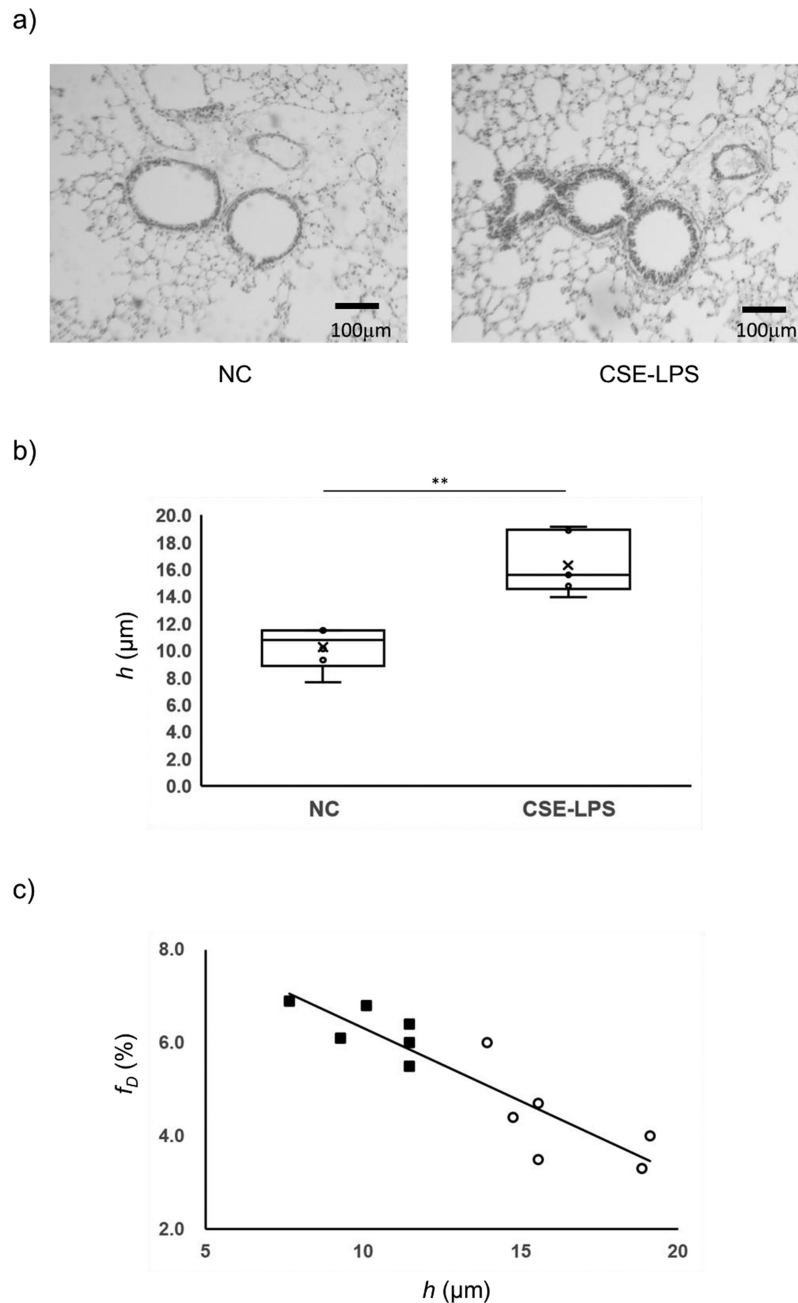


Fig. 4 Representative examples of histology slides obtained from NC and CSE-LPS mice (a), box plots of comparison of bronchial wall thickness (h) of the NC and CSE-LPS mice (b) (**: $P < 0.01$), and correlation between the bronchial wall thickness (h) and f_D ($r^2 = 0.81$ and $P < 0.01$). CSE-LPS, cigarette smoke extract and lipopolysaccharide; NC, negative control.

As mentioned above, the α value is apparently increased in the mild COPD onset but then ultimately decreased as the lung function declined further due to severe symptoms. To further support this hypothesis, we investigated the relationship between f_D and F_i and f_D and T_{1i} . A positive correlation was observed between f_D and F_i in CSE-LPS group, while no correlation was observed in the NC group (Fig. 6). Regarding the relationship between f_D and T_{1i} , inverse relationships

were observed in the CSE-LPS group and the NC group (Fig. 7). That is, a negative correlation was observed in the CSE-LPS group, whereas a positive correlation was observed in the NC group. These observations suggest a possible difference in oxygen metabolism between the CSE-LPS group and the NC group. In other words, when f_D increased in the NC group, oxygen uptake in the lungs might also increase, resulting in a possible concurrent increase

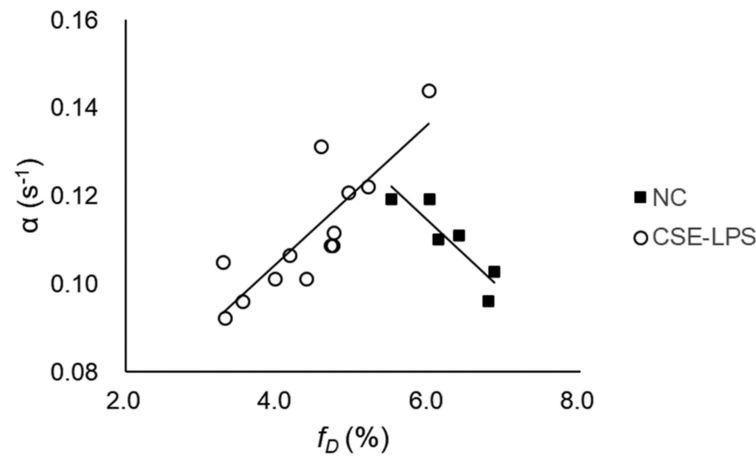


Fig. 5 Relationship between α and f_D of NC and CSE-LPS groups. Correlation: $r^2 = 0.71$ and $P < 0.01$ for the CSE-LPS mice, $r^2 = 0.79$ and $P < 0.01$ for the NC mice. CSE-LPS, cigarette smoke extract and lipopolysaccharide; NC, negative control.

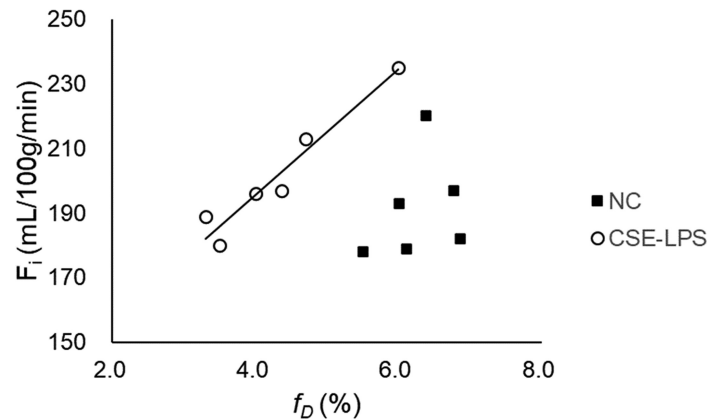


Fig. 6 Relationship between F_i and f_D of NC and CSE-LPS groups. Correlation: $r^2 = 0.93$ and $P < 0.01$ for the CSE-LPS mice, $r^2 = 0.09$ and $P > 0.05$ for the NC mice. CSE-LPS, cigarette smoke extract and lipopolysaccharide; NC, negative control.

of oxygenated blood. Due to the longer T_1 of ^{129}Xe dissolved in oxygenated blood (5.3s) than that in deoxygenated blood (1.2s),⁴⁰ T_{1i} is considered to be prolonged (Fig. 7). For our data, F_i did not correlate with f_D as a surrogate of oxygen uptake (Fig. 6). Reproducibility of FAIR measurements has been reported to be 1.8% intra-subject error and 15% inter-subject error for renal perfusion quantification.⁴¹ Therefore, the distribution of F_i of NC mice in the present study is likely somewhat attributable to inter mouse biological variability.

In contrast, when f_D increased in the CSE-LPS group, F_i also increased (Fig. 6), and the increase of F_i led to shortening of T_{1i} (Figure S2c). In other words, in the mild COPD with larger f_D , F_i could be increased (this is supported by two reports^{14,42} that mild COPD patients had significantly higher or preserved cerebral blood flow compared to healthy subjects). Nevertheless, oxygen uptake in the lung might not change exactly as indicated by f_D so that T_{1i} could be shortened as a result of increased deoxygenated blood. On the

other hand, in the severe COPD where f_D was reduced, F_i was also reduced (Fig. 6). This observation is supported by a report that moderate-to-severe COPD patients had significantly decreased cerebral blood flow compared to healthy subjects.¹⁴ In addition, it has been reported that in healthy subjects, the cerebral blood flow increased with short-term hypoxic challenge (20 mins) and decreased with long-term hypoxic challenge (2 hr and 10 hr) due to prolonged hypoxia.^{43,44} There is also a report that cerebral blood flow decreased in hypoxemic COPD patients.¹¹ Therefore, we can propose that F_i of the CSE-LPS mice decreased at this stage due to long-term smoking effect⁴⁵ (Fig. 6), as such the brain tissue became hypoxic although it remains to be seen how the balance between oxygenated and deoxygenated blood changes in severe COPD.⁴⁶ When the brain tissue became hypoxic, the oxygen concentration in the brain tissue decreased, likely resulting in a decrease in the effect of paramagnetic relaxation brought about by oxygen molecules

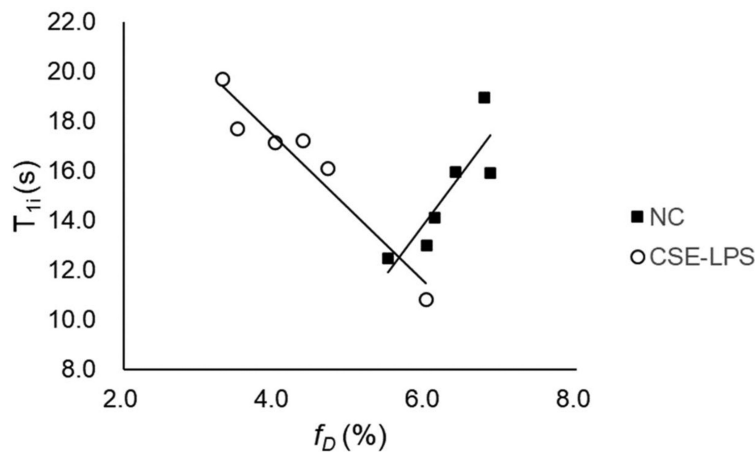


Fig. 7 Relationship between T_{1i} and f_D of NC and CSE-LPS groups. Correlation: $r^2 = 0.92$ and $P < 0.01$ for the CSE-LPS mice, $r^2 = 0.75$ and $P < 0.05$ for the NC mice. CSE-LPS, cigarette smoke extract and lipopolysaccharide; NC, negative control.

and a prolongation of T_{1i} . This is supported by a report that the direct interaction between oxygen molecules and HP ^{129}Xe in blood foam shortened the T_1 of HP ^{129}Xe due to paramagnetism of oxygen.⁴⁷ Furthermore, in this report, the effect of paramagnetism of oxygen molecules was more dominant than that of the relaxation caused by deoxygenated blood. Therefore, we can propose that in the present study, a decrease in the concentration of oxygen in brain tissue prolonged T_{1i} of HP ^{129}Xe diffused into brain tissue (Fig. 7) while the relative contribution of deoxygenated blood to the T_{1i} was small.

Consideration of other factors which influence brain uptake dynamics of HP ^{129}Xe

In Eqs. (3) and (4), brain uptake dynamics of HP ^{129}Xe depends not only on f_D but also on V_A/V_S . As there was no difference in MLI between the CSE-LPS and NC mice, α is unlikely dependent on V_A/V_S in the present study. Another factor that can influence α is the partition coefficient λ_i , which is assumed constant. Xe is fat-soluble and is a tracer that freely diffuses into the brain tissue. Therefore, it is considered that a change in the partition coefficient would not occur unless the brain volume is significantly changed, that is, the brain tissue is significantly destroyed, or the brain composition is altered. Although changes in brain structure and tissue such as a decrease in gray and white matter volume due to COPD have been reported,^{4–9,48,49} it is unlikely that the partition coefficient changed in this study.

Limitations

A major limitation of our work is the low number of data-points that were available for ^1H ASL for comparison with our ^{129}Xe measurements, which constrains the interpretation of the correlation analyses in Figs. 6 and 7. In addition, the

relationship between pulmonary gas exchange function and PaO_2 was not investigated. In fact, there are a few reports that PaO_2 was correlated with regional volume change induced in brain atrophy.^{8,9} Accordingly, it is challenging to explain the exact mechanisms of the change in cerebral oxygen metabolism due to lung damage in the COPD model mice. Direct measurements of PaO_2 and HP ^{129}Xe MRI/MRS would help to further clarify our hypothesis that the α and T_{1i} change reflecting cerebral oxygen metabolism change induced in the propagation of dysfunction from early phase to the chronic phase of the lung pathology.

Conclusion

By measuring pulmonary gas exchange function and brain uptake metrics using HP ^{129}Xe MRI/MRS, the relationship between lung function and brain tissue metabolism in a mouse model of COPD was investigated. In particular, we have derived the longitudinal relaxation time, T_{1i} , of HP ^{129}Xe in the brain tissue from the rate constant, α , of HP ^{129}Xe in the brain and the gCBF, and used it as a metric of brain tissue metabolism. In this CSE-LPS mouse model of COPD, by analyzing the interrelation between lung function and brain tissue metabolism, we have obtained preliminary insights into changes in cerebral oxygen metabolism during the transition from mild to severe pathology. In the future, this method may be useful in elucidating the pathogenic mechanism of brain dysfunction in comorbidities of COPD.

Acknowledgments

The authors are grateful to all the members of Department of Medical Physics and Engineering, Area

of Medical Imaging Technology and Science, Division of Health Sciences, Graduate School of Medicine, Osaka University, for their valuable comments and helpful discussions.

Funding

This work was supported in part by Grant-in-Aids of Scientific Research No. 20H04516, from the Ministry of Education, Culture, Science, Sports, and Technology of Japan.

Conflicts of Interest

The authors declare that they have no conflicts of interest.

References

- Barnes PJ. Chronic obstructive pulmonary disease: Effects beyond the lungs. *PLoS Med* 2010; 7:e1000220.
- Zhang J, Chen J, Yu Q, et al. Alteration of spontaneous brain activity in COPD patients. *Int J Chron Obstruct Pulmon Dis* 2016; 11:1713–1719.
- Xin H, Li H, Yu H, et al. Disrupted resting-state spontaneous neural activity in stable COPD. *Int J Chron Obstruct Pulmon Dis* 2019; 14:499–508.
- Spilling CA, Bajaj MK, Burrage DR, et al. Contributions of cardiovascular risk and smoking to chronic obstructive pulmonary disease (COPD)-related changes in brain structure and function. *Int J Chron Obstruct Pulmon Dis* 2019; 14:1855–1866.
- Yin M, Wang H, Hu X, Li X, Fei G, Yu Y. Patterns of brain structural alteration in COPD with different levels of pulmonary function impairment and its association with cognitive deficits. *BMC Pulm Med* 2019; 19:203.
- Taki Y, Kinomura S, Ebihara S, et al. Correlation between pulmonary function and brain volume in healthy elderly subjects. *Neuroradiology* 2013; 55:689–695.
- Sachdev PS, Anstey KJ, Parslow RA, et al. Pulmonary function, cognitive impairment and brain atrophy in a middle-aged community sample. *Dement Geriatr Cogn Disord* 2006; 21:300–308.
- Chen J, Lin IT, Zhang H, et al. Reduced cortical thickness, surface area in patients with chronic obstructive pulmonary disease: A surface-based morphometry and neuropsychological study. *Brain Imaging Behav* 2016; 10:464–476.
- Li J, Fei GH. The unique alterations of hippocampus and cognitive impairment in chronic obstructive pulmonary disease. *Respir Res* 2013; 14:140.
- Van de Ven MJ, Colier WN, Van der Sluijs MC, Kersten BT, Oeseburg B, Folgering H. Ventilatory and cerebrovascular responses in normocapnic and hypercapnic COPD patients. *Eur Respir J* 2001; 18:61–68.
- Ortapamuk H, Naldoken S. Brain perfusion abnormalities in chronic obstructive pulmonary disease: Comparison with cognitive impairment. *Ann Nucl Med* 2006; 20:99–106.
- Yildiz S, Kaya I, Cece H, et al. Impact of COPD exacerbation on cerebral blood flow. *Clin Imaging* 2012; 36:185–190.
- Beaudin AE, Hartmann SE, Pun M, Poulin MJ. Human cerebral blood flow control during hypoxia: Focus on chronic pulmonary obstructive disease and obstructive sleep apnea. *J Appl Physiol* 2017; 1350–1361.
- Wijnant SRA, Bos D, Brusselle G, et al. Comparison of cerebral blood flow in subjects with and without chronic obstructive pulmonary disease from the population-based Rotterdam Study. *BMJ Open* 2021; 11:e053671.
- Kern AL, Vogel-Claussen J. Hyperpolarized gas MRI in pulmonology. *Br J Radiol* 2018; 91:20170647.
- Shepelytskyi Y, Grynko V, Rao MR, et al. Hyperpolarized ^{129}Xe imaging of the brain: Achievements and future challenges. *Magn Reson Med* 2022; 88:83–105.
- Imai H, Kimura A, Akiyama K, Ota C, Okimoto K, Fujiwara H. Development of a fast method for quantitative measurement of hyperpolarized ^{129}Xe dynamics in mouse brain. *NMR Biomed* 2012; 25:210–217.
- Hane FT, Li T, Plata JA, Hassan A, Granberg K, Albert MS. Inhaled xenon washout as a biomarker of Alzheimer's disease. *Diagnostics (Basel)* 2018; 8:41.
- Rao MR, Stewart NJ, Griffiths PD, Norquay G, Wild JM. Imaging human brain perfusion with inhaled hyperpolarized ^{129}Xe MR imaging. *Radiology* 2018; 286:659–665.
- Shepelytskyi Y, Hane FT, Grynko V, Li T, Hassan A, Albert MS. Hyperpolarized ^{129}Xe time-of-flight MR imaging of perfusion and brain function. *Diagnostics (Basel)* 2020; 10:630.
- Li H, Zhang Z, Zhong J, et al. Oxygen-dependent hyperpolarized ^{129}Xe brain MR. *NMR Biomed* 2016; 29:220–225.
- Kimura A, Wakayama T, Narazaki M, Kawata Y, Ueyama T, Fujiwara H. Improvement of T_1 determination of hyperpolarized ^{129}Xe in mouse brain under controlled-flow. *Magn Reson Med Sci* 2004; 3:199–205.
- Kimura A, Imai H, Wakayama T, Fujiwara H. A simple method for quantitative measurement and analysis of hyperpolarized ^{129}Xe uptake dynamics in mouse brain under controlled flow. *Magn Reson Med Sci* 2008; 7:179–185.
- Kimura A, Yamauchi Y, Hodono S, et al. Treatment response of ethyl pyruvate in a mouse model of chronic obstructive pulmonary disease studied by hyperpolarized ^{129}Xe MRI. *Magn Reson Med* 2017; 78:721–729.
- Ruppert K, Brookeman JR, Hagspiel KD, Mugler JP 3rd. Probing lung physiology with xenon polarization transfer contrast (XTC). *Magn Reson Med* 2000; 44:349–357.
- Peled S, Jolesz FA, Tseng CH, Nascimben L, Albert MS, Walsworth RL. Determinants of tissue delivery for ^{129}Xe magnetic resonance in humans. *Magn Reson Med* 1996; 36:340–344.
- Ruppert K, Mata JF, Brookeman JR, Hagspiel KD, Mugler JP 3rd. Exploring lung function with hyperpolarized ^{129}Xe nuclear magnetic resonance. *Magn Reson Med* 2004; 51:676–687.
- Mizutani N, Fuchikami J, Takahashi M, Nabe T, Yoshino S, Kohno S. Pulmonary emphysema induced by cigarette smoke solution and lipopolysaccharide in guinea pigs. *Biol Pharm Bull* 2009; 32:1559–1564.
- Imai H, Kimura A, Iguchi S, Hori Y, Masuda S, Fujiwara H. Noninvasive detection of pulmonary tissue destruction in a mouse model of emphysema using hyperpolarized ^{129}Xe MRS

- under spontaneous respiration. *Magn Reson Med* 2010; 64:929–938.
30. Nakamura K, Kondoh Y, Wakai A, Kershaw J, Wright D, Kanno I. ^{129}Xe spectra from the heads of rats with and without ligation of the external carotid and pterygopalatine arteries. *Magn Reson Med* 2005; 53:528–534.
 31. Pell GS, Thomas DL, Lythgoe MF, et al. Implementation of quantitative FAIR perfusion imaging with a short repetition time in time-course studies. *Magn Reson Med* 1999; 41:829–840.
 32. Duhamel G, Callot V, Cozzone PJ, Kober F. Spinal cord blood flow measurement by arterial spin labeling. *Magn Reson Med* 2008; 59:846–854.
 33. Herscovitch P, Raichle ME. What is the correct value for the brain—blood partition coefficient for water? *J Cereb Blood Flow Metab* 1985; 5:65–69.
 34. Narazaki M, Kimura A, Wakayama T, Imai H, Fujiwara H. Origin of dissolved-phase hyperpolarized ^{129}Xe signal in the mouse chest based on experimental evidence from extensive magnetic resonance measurements. *Magn Reson Med Sci* 2011; 10:149–154.
 35. Chen RY, Fan FC, Kim S, Jan KM, Usami S, Chien S. Tissue-blood partition coefficient for xenon: Temperature and hematocrit dependence. *J Appl Physiol* 1980; 49:178–183.
 36. Gellner CA, Reynaga DD, Leslie FM. Cigarette smoke extract: A preclinical model of tobacco dependence. *Curr Protoc Neurosci* 2016; 77:9.54.1–9.54.10.
 37. Wolber J, Cherubini A, Leach MO, Bifone A. On the oxygenation-dependent ^{129}Xe T_1 in blood. *NMR Biomed* 2000; 13:234–237.
 38. Albert MS, Balamore D, Kacher DF, Venkatesh AK, Jolesz FA. Hyperpolarized ^{129}Xe T_1 in oxygenated and deoxygenated blood. *NMR Biomed* 2000; 13:407–414.
 39. Wolber J, Cherubini A, Leach MO, Bifone A. Hyperpolarized ^{129}Xe NMR as a probe for blood oxygenation. *Magn Reson Med* 2000; 43:491–496.
 40. Norquay G, Leung G, Stewart NJ, Tozer GM, Wolber J, Wild JM. Relaxation and exchange dynamics of hyperpolarized ^{129}Xe in human blood. *Magn Reson Med* 2015; 74:303–311.
 41. Harteveld AA, de Boer A, Franklin SL, Leiner T, van Stralen M, Bos C. Comparison of multi-delay FAIR and pCASL labeling approaches for renal perfusion quantification at 3T MRI. *MAGMA* 2020; 33:81–94.
 42. Bernardi L, Casucci G, Haider T, et al. Autonomic and cerebrovascular abnormalities in mild COPD are worsened by chronic smoking. *Eur Respir J* 2008; 32:1458–1465.
 43. Harris AD, Murphy K, Diaz CM, et al. Cerebral blood flow response to acute hypoxic hypoxia. *NMR Biomed* 2013; 26:1844–1852.
 44. Lawley JS, Macdonald JH, Oliver SJ, Mullins PG. Unexpected reductions in regional cerebral perfusion during prolonged hypoxia. *J Physiol* 2017; 595:935–947.
 45. Yamashita K, Kobayashi S, Yamaguchi S, Kitani M, Tsunematsu T. Effect of smoking on regional cerebral blood flow in the normal aged volunteers. *Gerontology* 1988; 34:199–204.
 46. Tariq S, Ismail D, Thapa M, et al. Chronic obstructive pulmonary disease and its effect on red blood cell indices. *Cureus* 2023; 15:e36100.
 47. Tseng CH, Peled S, Nascimben L, Oteiza E, Walsworth RL, Jolesz FA. NMR of laser-polarized ^{129}Xe in blood foam. *J Magn Reson* 1997; 126:79–86.
 48. Zhang H, Wang X, Lin J, et al. Reduced regional gray matter volume in patients with chronic obstructive pulmonary disease: A voxel-based morphometry study. *AJNR Am J Neuroradiol* 2013; 34:334–339.
 49. Dodd JW, Chung AW, van den Broek MD, Barrick TR, Charlton RA, Jones PW. Brain structure and function in chronic obstructive pulmonary disease: A multimodal cranial magnetic resonance imaging study. *Am J Respir Crit Care Med* 2012; 186:240–245.